Medical Physics
The International Journal of Medical Physics Research and Practice

First evaluation of the feasibility of MLC tracking using ultrasound motion estimation

Martin F. Fast, Tuathan P. O'Shea, Simeon Nill, Uwe Oelfke, and Emma J. Harris

Citation: Medical Physics **43**, 4628 (2016); doi: 10.1118/1.4955440
View online: http://dx.doi.org/10.1118/1.4955440
View Table of Contents: http://scitation.aip.org/content/aapm/journal/medphys/43/8?ver=pdfcov
Published by the American Association of Physicists in Medicine

First evaluation of the feasibility of MLC tracking using ultrasound motion estimation

Martin F. Fast,[a),b)] Tuathan P. O'Shea,[b),c)] Simeon Nill, Uwe Oelfke, and Emma J. Harris
Joint Department of Physics, The Institute of Cancer Research and The Royal Marsden NHS Foundation Trust, London SM2 5NG, United Kingdom

(Received 11 February 2016; revised 21 June 2016; accepted for publication 25 June 2016; published 18 July 2016)

Purpose: To quantify the performance of the Clarity ultrasound (US) imaging system (Elekta AB, Stockholm, Sweden) for real-time dynamic multileaf collimator (MLC) tracking.
Methods: The Clarity calibration and quality assurance phantom was mounted on a motion platform moving with a periodic sine wave trajectory. The detected position of a 30 mm hypoechogenic sphere within the phantom was continuously reported via Clarity's real-time streaming interface to an in-house tracking and delivery software and subsequently used to adapt the MLC aperture. A portal imager measured MV treatment field/MLC apertures and motion platform positions throughout each experiment to independently quantify system latency and geometric error. Based on the measured range of latency values, a prostate stereotactic body radiation therapy (SBRT) delivery was performed with three realistic motion trajectories. The dosimetric impact of system latency on MLC tracking was directly measured using a 3D dosimeter mounted on the motion platform.
Results: For 2D US imaging, the overall system latency, including all delay times from the imaging and delivery chain, ranged from 392 to 424 ms depending on the lateral sector size. For 3D US imaging, the latency ranged from 566 to 1031 ms depending on the elevational sweep. The latency-corrected geometric root-mean squared error was below 0.75 mm (2D US) and below 1.75 mm (3D US). For the prostate SBRT delivery, the impact of a range of system latencies (400–1000 ms) on the MLC tracking performance was minimal in terms of gamma failure rate.
Conclusions: Real-time MLC tracking based on a noninvasive US input is technologically feasible. Current system latencies are higher than those for x-ray imaging systems, but US can provide full volumetric image data and the impact of system latency was measured to be small for a prostate SBRT case when using a US-like motion input. [http://dx.doi.org/10.1118/1.4955440]

Key words: ultrasound, multileaf collimator, MLC, real-time tumor tracking, motion management

1. INTRODUCTION

Real-time dynamic multileaf collimator (MLC) tracking is an emerging adaptive radiation therapy (RT) delivery technique aimed at increasing dose conformity to the target by reshaping the plan segment, i.e., MLC aperture, to the most recently observed target position. MLC tracking is not only able to compensate for intrafractional motion, but also implicitly for residual interfractional setup errors which occur even after performing modern image-guided radiation therapy. The accuracy and timeliness (i.e., latency) of target position data are paramount to successful tracking. The dosimetric improvements provided by MLC tracking of the prostate during irradiation have been illustrated for a range of fractionation schedules.[1] Colvill *et al.* demonstrated that although the impact of intrafractional prostate motion averaged over the entire patient cohort was found to be small, systematic drifts and/or sudden transient motion events can lead to outlier fractions resulting in under-dosed targets. This is especially of concern for hypofractionated stereotactic body radiation therapy (SBRT) delivery schedules and reduced margins.[2]

Prostate SBRT treatment regimes are advantageous from a health economics and patient comfort point of view due to the drastically reduced number of treatment fractions and thus hospital visits. From a radiobiological point of view, the prostate also lends itself to hypofractionation as the linear–quadratic model predicts an improvement in the therapeutic ratio with a reduced number of fractions since the α/β ratio for prostate cancer is lower than the α/β ratio for late rectal toxicity (the main dose constraint).[3] For SBRT, individual fractions which exhibit larger motion and potential under-dosage of the target are not "averaged out" over the small number of total fractions encompassing the entire treatment delivery, motivating the need for active motion management.

A variety of mostly ionizing and/or invasive target detection modalities for intrafractional motion management has been discussed in the literature.[1,4,5] Ultrasound (US) imaging is a potential alternative method for providing intrafractional positional information to guide the MLC during RT.[6] US imaging is nonionizing and noninvasive, and it provides soft-tissue detail and has the ability to provide high frame (2D) or

volume rates (3D).[7] In this study, we report on the first use of the Clarity US imaging system (Elekta AB, Stockholm, Sweden) for MLC-based motion tracking. To this effect, Clarity is integrated with an in-house developed tracking and delivery software for the Elekta Agility MLC.[8]

The Clarity system provides interfractional set-up corrections by integrating US at the patient simulation and treatment platform.[9] 3D ultrasound volumes are registered to the isocenter in both the simulator and treatment rooms. The device can also perform intrafraction monitoring during radiation delivery with 3D images acquired via the perineum. Based on a previously established measurement protocol,[8] this study investigates overall system latency and geometric tracking error for a range of 2D/3D imaging settings. The various latency contributions and US motion estimation errors are calculated from Clarity log files. The dosimetric impact of measured latencies on the MLC tracking performance is illustrated by delivering a clinical prostate SBRT plan to a 3D dosimeter.

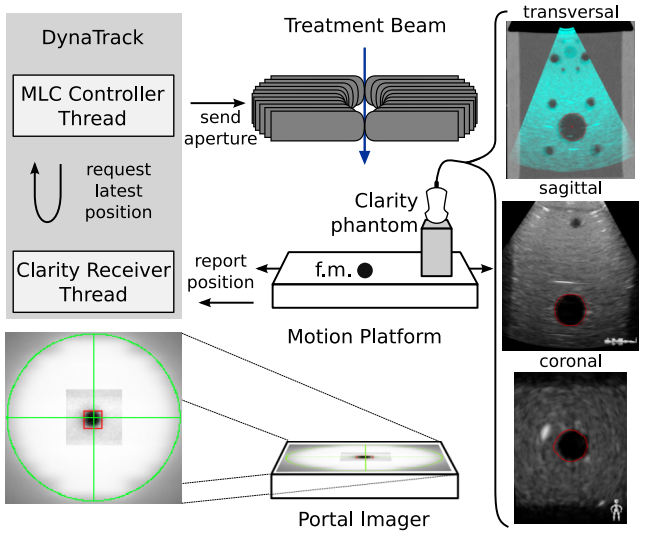

FIG. 1. Schematic representation of the experimental setup (not to scale) used for measuring system latency and geometric tracking error (cf. Fig. 1 in Ref. 8): fiducial marker (f.m.) and treatment beam are both visible on the portal imager. Sample US images are shown on the right. The transversal US image (blue color wash) is shown registered to the planning CT image of the phantom.

2. MATERIALS AND METHODS

2.A. Dynamic MLC tracking

Dynamic real-time MLC tracking for the Agility MLC was introduced in a previous study.[8] Subsequently, *DynaTrack*—the in-house developed tracking and delivery software interfaced to the Agility MLC / Synergy linac via real-time research interfaces provided by Elekta—was extended to tracked VMAT (Ref. 10) and step-and-shoot IMRT deliveries (Ref. 2). In the previous studies, MLC tracking was informed by high-frequency position detection devices, either directly by motion platform position encoders or by a simulated electromagnetic beacon-type (e.g., Calypso) input device. In either case, position updates were provided at a frequency similar to the update rate of the MLC (25 Hz), leading to continuous MLC motion. In this study, however, the lower position update rate of the Clarity US device ($\leq$5 Hz) required a complete rewrite of the central MLC controller thread (Fig. 1) which is responsible for sending updated MLC apertures to the MLC based on the most recently detected target position. Since MLC adjustment is now much quicker than the time between position updates, the net effect is a "stop-and-go" tracking mode, similar to the work performed by Poulsen *et al.*,[4] in which the MLC comes to a standstill once a new target position is adapted to and no new target position is available.

2.B. Experimental setup

The experimental setup used to investigate the performance of Clarity US-based MLC tracking is shown in Fig. 1. The main components were a high-precision 4D motion platform (0.2 mm accuracy[11]) which was moved by a 1D superior–inferior (SI) sine wave trajectory (20 mm peak-to-peak, 5 s period) and the portal imager which independently monitored the motion platform (i.e., a circular fiducial marker) and MV treatment field trajectories.[8] To avoid any impact of the MLC leaf speed limitation on the measurements, the MLC was rotated to 90° to align the leaf travel direction with the SI motion. It was previously shown that target motion orthogonal to the leaf travel direction introduces an extra 10–15 ms delay on the Agility MLC.[8] For this study, the Clarity calibration and quality assurance (QA) phantom was also placed on the motion platform. The Autoscan transducer, supported by a rigid mechanical arm (Manfrotto™, Italy) and attached to the treatment couch, was positioned above the QA phantom. Water was used as an acoustic couplant between the phantom and transducer and to enable motion of the phantom relative to the transducer.

2.C. Clarity ultrasound monitoring

The Clarity calibration and QA phantom which contains a 30 mm hypoechogenic sphere at 115 mm depth was imaged with a 5 MHz abdominal Autoscan transducer (m4DC7-3/40, Elekta Ltd.). A single 3D US image was registered with a previously acquired CT image of the phantom in the Clarity Automatic Fusion and Contouring (AFC) generation 4 software (AntiCosti 2015, Elekta Ltd.) and a 3D reference positional volume (RPV) was generated based on the contour of the 30 mm sphere in US images. Following export to the Clarity US scanner, the CLARITY GUIDE software was used to setup and monitor the position of the RPV center-of-mass as the phantom underwent motion. The Clarity Experimental Monitoring (CEM) module, which permits the operator to access imaging settings and stream monitoring data (only available in research mode), was used to image the phantom and send estimated RPV centroid motion to *DynaTrack*. During intrafraction motion monitoring, the mechanically swept Clarity transducer continuously scans a 3D volume (or a single 2D frame with no mechanical sweep) and the system estimates the rigidly shifted position of the RPV with

TABLE I. US imaging settings used in this study. The imaging rate is inversely proportional to the sector size (2D) and elevational sweep (3D). The fields-of-view (FOVs) are calculated at the depth of the sphere in the QA phantom (115 mm).

	2D	3D
Sector size (deg)	39.5–79	39.5
Sector FOV (mm)	111–255	111
Elevational sweep (deg)	0	3.6–20.8
Elevational FOV (mm)	0	8–49
Line density	192	64
Depth (mm)	150	150
Imaging rate (Hz)	47–23	13.3–2.5

a normalized cross correlation-based algorithm optimized for low velocity prostate trajectories. The transducer position is optically tracked within the treatment room (Polaris Spectra, NDI, Canada) with an Elekta-devised calibration procedure relating each US pixel to a corresponding position in room coordinates. Further details on the intrafraction monitoring algorithm are contained in the work of Lachaine and Falco.[9] It should be noted that the motion estimation algorithms in Clarity were designed for prostate, i.e., using Clarity for detecting sinusoidal motion, as necessary for this study, is outside of vendor intended operating parameters.

In the current study, the ultrasound transducer sweep (elevational) axis was aligned with the right–left (RL) axis, while the lateral axis was aligned with the direction of motion (SI). The CEM module was used to investigate the effect of various 2D and 3D imaging parameters (Table I) on the total system latency. Additionally, the amplitude and period of the sine wave trajectory were varied for one of the 2D US imaging settings (sector size: 59.3°) to investigate the possible impact of maximum target speed on system latency.

2.D. Definitions: Latency and geometric tracking error

System latency τ_{sys} was defined as the overall time delay between when a new target position was realized and when the MLC was fully adapted to it. It included contributions from both the Clarity and the Agility systems. From Poulsen *et al.*,[4] we adopt the following notation for system latency:

$$\tau_{sys} = \langle T_{US} \rangle + 0.5 \times \langle \Delta T_{image} \rangle + 0.5 \times \langle \tau_{MLC} \rangle. \quad (1)$$

T_{US} is the latency contribution of the Clarity system including image acquisition, motion estimation, and the transfer of the detected target position to *DynaTrack*. $\langle \Delta T_{image} \rangle$ is the inverse position update rate of the Clarity system, i.e., the average time interval between new position estimates (not to be confused with the inverse imaging rate). It is calculated from log files saved during monitoring by the CEM module containing system timestamped displacement data points. $0.5 \times \langle \Delta T_{image} \rangle$ corresponds to the mean waiting time between a change in target position and its observation by the Clarity system. $\langle \tau_{MLC} \rangle$ is the mean MLC adjustment latency, i.e., the time delay between requesting a new MLC position and reaching it.

To exclude the effect of system latency on geometric tracking error, the latency-corrected (τ-less) root-mean squared error is defined as follows:

$$\mathrm{RMSE}_{\tau\text{-less}} = \sqrt{\frac{1}{N}\sum_{t=t_1}^{t_N}\left(s^{fm}(t) - s^{field}\left(t+\tau_{sys}\right)\right)^2}. \quad (2)$$

Here, N denotes the number of data points, $s^{fm} = (0, y_{SI}, 0)^T$ the motion platform (i.e., fiducial marker) trajectory as a function of time t, and s^{field} the latency-corrected center-of-mass trajectory of the MV treatment field (s in IEC 61217 coordinates). Excluding the effect of latency effectively assumes perfect motion prediction[12] and is thus an idealized scenario. It is nonetheless instructive, as it allows us to isolate the error contributions of Clarity's motion estimation algorithm, the effect of under-sampling the motion, and the MLC leaf adjustments. System latency [Eq. (1)] and geometric tracking error [Eq. (2)] are measured by automatically identifying s^{fm} and s^{field} directly from the sequence of portal images acquired during each experiment.[8] The system latency corresponds to the phase shift between the sine wave trajectories fitted to the motion platform and MV treatment field trajectories, respectively. The geometric tracking error corresponds to the (averaged) latency-corrected geometric distance of the two trajectories. The accuracy of the motion platform, RMSE_{MP}, was validated for each run by comparing the imager-derived motion platform trajectory s^{fm} with the input trajectory sent to the platform. A subset of these measurements was repeated with a load of 24 kg, equivalent to the weight of the 3D dosimeter (described below in Sec. 2.E).

To further quantify the motion estimation error of the Clarity system, RMSE_{US} was calculated for the realistic 3D prostate trajectories (cf. Sec. 2.E) by comparing the (latency-corrected) target positions reported by Clarity with the motion platform trajectories. For the prostate trajectories, this was done using the CIRS Model 053 US prostate phantom (CIRS, Inc., Norfolk, USA), submerged in a water container, to allow for full 3D motion with the transducer remaining stationary.

2.E. Dosimetric impact of US-based MLC tracking

To assess the dosimetric impact of a range of different system latencies (400, 600, and 1000 ms) for a typical prostate SBRT patient (PTV = 104 cc, RTOG 0938 planning guidelines, 6 MV, 7 equidistant beams, 2° collimator), an additional verification experiment was performed. The Delta^4 diode array (Scandidos, Uppsala, Sweden)[13] was placed on the motion platform previously used for the Clarity phantom. Three different delivery and motion scenarios were tested: (i) static—no motion/no tracking, (ii) conventional—motion/no tracking, and (iii) tracked—motion/tracking. Three different previously recorded motion traces were used: a baseline drift posteriorly and inferiorly (*continuous drift*), a baseline drift posteriorly and inferiorly with sudden transient motion mostly anteriorly (*erratic*), and a slow baseline drift anteriorly and superiorly with sudden transient motion anteriorly and superiorly (*high frequency*).[2] All traces were normalized to start at the isocenter. The 400 s motion traces were used as inputs for the motion

platform. Direct 3D US monitoring was not deemed feasible in this setup as we could not simultaneously accommodate the Delta[4] and the US phantom on the motion platform due to space limitations. Instead, actually achieved platform positions, as measured by the internal position encoders of the motion platform, were reported to *DynaTrack* via a direct UDP network link.[8] These target positions were then artificially queued in *DynaTrack* to achieve the desired overall system latency.[10] Deliveries were reproducibly started within a few seconds from the beginning of the motion trace. Resulting 3D dose distributions were compared in the Delta[4] software by means of a global gamma analysis (1%/1 mm, 2%/2 mm and 3%/3 mm). For all cases, the measurement from the static delivery was used as reference dose distribution. The dose measured at the isocenter of the static delivery was used as a reference value for the gamma analysis and voxels below 10% of the reference value were excluded from the analysis.

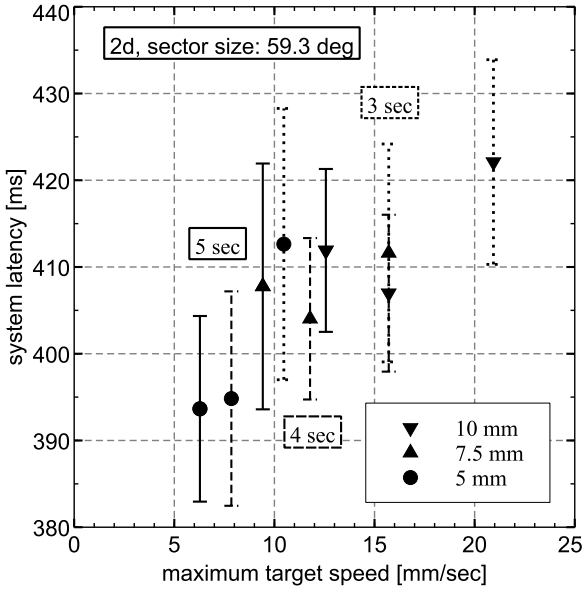

FIG. 3. System latency for US-based MLC tracking of different sine wave trajectories as a function of maximum target speed. Period is encoded by line style: 5 s (solid), 4 s (dashed), and 3 s (dotted).

3. RESULTS

3.A. Latency

Figure 2 summarizes the latency findings for all US imaging settings. $\langle T_{US} \rangle$ is calculated from Eq. (1) and assumes $\langle \tau_{MLC} \rangle = 30$ ms.[8] For the 2D acquisitions, system latency increases moderately with sector size. $\langle \Delta T_{image} \rangle$, as logged by the Clarity log files, appears to be independent of the sector size, suggesting that the average time between position updates calculated by Clarity is not affected by the increase in 2D US image size. The inverse imaging rate is below 50 ms for all sector sizes, indicating that motion estimation time is the main cause for delay on the imaging side. For the 3D acquisitions, system latency increases linearly ($R^2 = 0.94$) with elevational sweep. $\langle \Delta T_{image} \rangle$ increases strongly between ~3°–10° elevational sweep but appears to plateau for larger sweep angles despite the linear ($R^2 = 0.99$) increase in the inverse imaging rate. It should be noted that Clarity uses partially updated 3D volumes for position estimation and that Eq. (1) is derived for a scenario where the image acquisition time is much smaller than the inverse position update rate. For large sweep angles, this assumption is clearly violated.

Parameter selection for the sine trajectory has a visible impact on system latency (Fig. 3) as measured with one of the 2D US imaging settings. Neither amplitude nor period is a clear predictor for system latency, but the relationship between maximum target speed and system latency is weakly linear ($R^2 = 0.69$).

3.B. Geometric tracking error

Figure 4 highlights the different geometric errors derived from our experimental setup as a function of the US sector

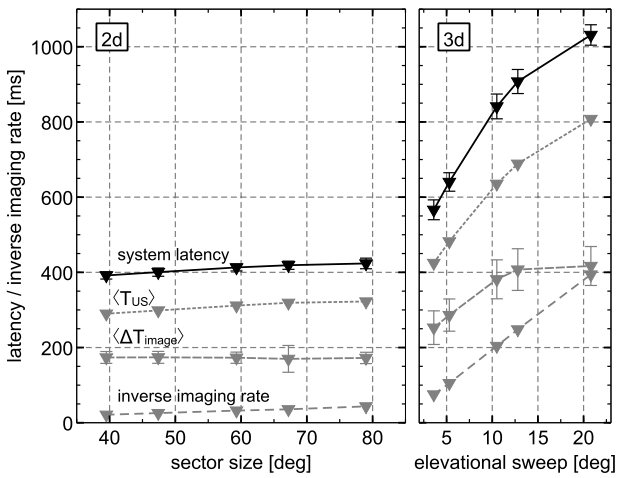

FIG. 2. System latency, its individual components [Eq. (1)], and inverse imaging rate for US-based MLC tracking of a sine wave trajectory as a function of US sector size (2D) and elevational sweep (3D).

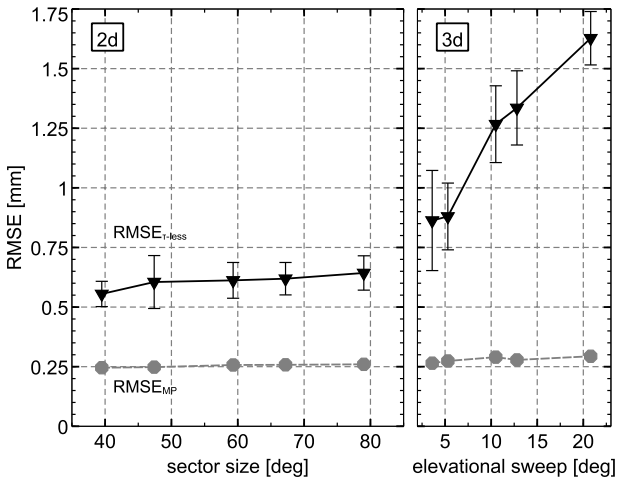

FIG. 4. Latency-corrected geometric tracking error ($RMSE_{\tau\text{-less}}$) and motion platform accuracy ($RMSE_{MP}$) for US-based MLC tracking of a sine wave trajectory as a function of US sector size (2D) and elevational sweep (3D).

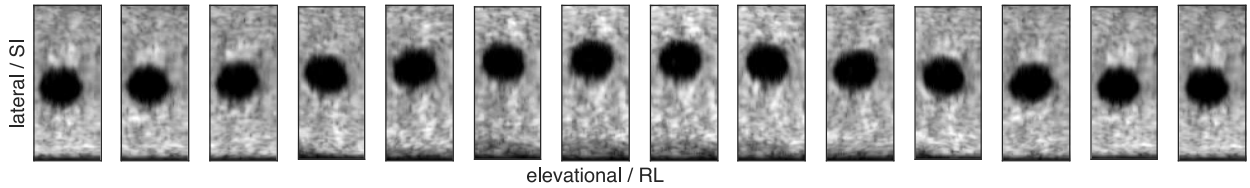

FIG. 5. Worst case geometric distortions during a full 5 s period as observed in the slowest 3D US acquisition (elevational sweep angle: 20.8°). The image size corresponds to the FOV at the depth of the sphere.

size and elevational sweep. For 2D acquisitions, the latency-corrected geometric displacement between fiducial marker and MV treatment field ($RMSE_{\tau\text{-less}}$) is shown to increase moderately with sector size. For 3D acquisitions, the increased latency also translates into a larger $RMSE_{\tau\text{-less}}$ compared to the 2D acquisition. Here, the tracking error increases linearly ($R^2 = 0.97$) with elevational sweep.

The accuracy of the motion platform ($RMSE_{MP}$) is measured to be <0.35 mm which essentially corresponds to the effective pixel resolution of the portal imager at the isocenter. The largest geometric mismatch between the motion platform input trajectory and actual trajectory occurred at the respiratory extrema where the platform tended to exceed the prescribed motion amplitude. As expected, $RMSE_{MP}$, which is estimated independently from the Clarity system, does not depend on the US imaging settings. Introducing an additional weight of 24 kg had no discernible impact on the accuracy of the motion platform.

The $RMSE_{US}$ averaged over all realistic 3D prostate trajectories (Sec. 2.E) was 0.7 ± 0.2 mm (2D US), 0.6 ± 0.1 mm (3D US, smallest elevational sweep), and 0.7 ± 0.2 mm (3D US, largest elevational sweep), respectively. For the 2D acquisitions, out-of-plane RL motion could not be resolved and produced the largest error contribution.

3.C. Geometric image distortions

For 3D US imaging with large elevational sweeps and thus correspondingly low imaging rates, there is a danger that interplay between target and transducer motion will lead to artifact-ridden images which could result in incorrectly assigned target positions.[14] By looking at a worst case scenario of 20.8° elevational sweep angle, we were able to quantify the image distortions in the lateral/elevational plane at an axial depth corresponding to the center of the hypoechogenic sphere (Fig. 5). Given the size of the spherical inclusion (30 mm), the elevational FOV (49 mm), the inverse imaging rate (394 ms), and a maximum target speed of 12.6 mm/s, a maximum distortion of 3 mm is expected between the opposing edges of the spherical inclusion. Using Otsu thresholding,[15] the inclusion area varied by 3.6% (mean) over the course of the entire period compared to the first image of the series. As expected, the maximum deviation (8.4%) occurred between the sinusoid extrema when target motion was at its maximum. The Dice similarity coefficient[16] was 0.94 ± 0.03 averaged over the entire period with the lowest score (0.91) occurring on the opposite extrema of the sinusoid.

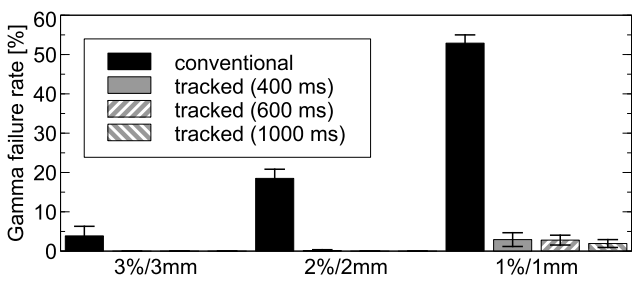

FIG. 6. Average gamma failure rate for three prostate motion trajectories. Some bars are zero and thus not visible.

3.D. Dosimetric impact of ultrasound-based tracking

The gamma failure rates for a typical prostate SBRT patient subject to either a conventional delivery or tracked deliveries (with different overall system latencies) based on three different motion trajectories are shown in Fig. 6. Regardless of the motion trajectory, the gamma failure of the conventional delivery increases dramatically when going from 3%/3 mm toward 1%/1 mm. For the tracked deliveries, the dosimetric effect of all investigated latencies appears minimal and the average gamma failure is around 2% at 1%/1 mm.

4. CONCLUSIONS

To our knowledge, this is the first experimental study demonstrating the feasibility of US motion estimation to guide dynamic MLC tracking on a research radiotherapy treatment platform. The overall system latency, including all delay times from the imaging and delivery chain, ranged from 392 to 424 ms (2D US) depending on lateral sector size and from 566 to 1031 ms (3D US) depending on elevational sweep. Varying the sine wave trajectory parameters (amplitude and period) introduced another small modulation to the latency. Similar to previous observations,[8] increases in the maximum target speed yielded increases in latency as well. The average latency-corrected tracking RMSE was below 0.75 mm (2D US) and below 1.75 mm (3D US). Fledelius *et al.*[17] have reported system latencies of 264 ms (382 ms) for kV (MV) x-ray based MLC tracking. While Clarity-based MLC tracking has a higher delay time, especially for 3D image acquisitions, US imaging is nonionizing and does not require implanted markers.

2D US allows for a faster response of the MLC to motion but it requires prior knowledge about the orientation of motion if out-of-plane motion is to be minimized. An exploratory analysis of latency-corrected US-only RMSE for three realistic

prostate trajectories confirmed that out-of-plane motion (in RL direction in this study) poses a challenge for 2D US imaging. When using 3D US imaging, employing even the smallest elevational sweep angle of 3.6° improved the RL resolution visibly.

Measuring latency requires a controlled and thus artificial experimental setup. Results should nevertheless be applicable to in-vivo patient imaging as long as the target can be reliably detected in the US images. In terms of geometric accuracy, the transition to in-vivo images is expected to have a greater impact due to the anticipated decrease in contrast compared to the relatively simple US phantoms employed in this study. Although beyond the scope of this study, the determination of position estimation accuracy in-vivo against a gold standard method such as x-ray imaging with fiducials needs to be addressed before any US-based MLC tracking system can be introduced into the clinic.

The potential dosimetric impact of a US-like range of system latencies (400–1000 ms) on the performance of MLC tracking was found to be minimal for a prostate SBRT case subject to three realistic motion conditions. MLC-based tracking for prostate SBRT with current 3D ultrasound transducer technology appears to be feasible but the intrafractional target detection accuracy needs to be validated with patient data. If US imaging was applied to organs dominated by respiratory motion (something the Clarity motion estimation algorithm is not optimized for in its current form), the latency and corresponding geometric beam-target misalignment would need to be reduced by speeding up image acquisition, motion estimation times. and/or employing motion prediction algorithms.[12] For comparatively slow 3D US acquisitions, the interplay between target and transducer mechanical sweep was shown to lead to small but measurable image distortions for a fast sine wave trajectory. One obvious solution to this problem could be the 2D matrix array transducer technology. Bell *et al.*[18] have reported on the use of such a probe without mechanically swept components for in-vivo liver imaging. For a 3D imaging volume (~14 cm×6 cm×7 cm) slightly smaller than the volume used in this study, they achieved an imaging rate of 24 Hz.

ACKNOWLEDGMENTS

The authors acknowledge support of the MLC tracking and ultrasound imaging research from Elekta AB under research agreements. M.F.F. is supported by Cancer Research UK under Programme No. C33589/A19908. Research at The Institute of Cancer Research is also supported by Cancer Research UK under Programme No. C33589/A19727 and NHS funding to the NIHR Biomedical Research Centre at The Royal Marsden and The Institute of Cancer Research.

CONFLICT OF INTEREST DISCLOSURE

The authors have no COI to report.

[a]Electronic mail: martin.fast@icr.ac.uk
[b]Martin F. Fast and Tuathan P. O'Shea contributed equally to this work.
[c]Electronic mail: tuathan.oshea@nhs.net

[1]E. Colvill, J. T. Booth, R. T. O'Brien, T. N. Eade, A. B. Kneebone, P. R. Poulsen, and P. J. Keall, "Multileaf collimator tracking improves dose delivery for prostate cancer radiation therapy: Results of the first clinical trial," Int. J. Radiat. Oncol., Biol., Phys. **92**(5), 1141–1147 (2015).
[2]M. F. Fast, C. P. Kamerling, P. Ziegenhein, M. J. Menten, J. L. Bedford, S. Nill, and U. Oelfke, "Assessment of MLC tracking performance during hypofractionated prostate radiotherapy using real-time dose reconstruction," Phys. Med. Biol. **61**(4), 1546–1562 (2016).
[3]D. Henderson, A. Tree, and N. van As, "Stereotactic body radiotherapy for prostate cancer," Clin. Oncol. **27**(5), 270–279 (2015).
[4]P. R. Poulsen, B. Cho, A. Sawant, D. Ruan, and P. J. Keall, "Detailed analysis of latencies in image-based dynamic MLC tracking," Med. Phys. **37**(9), 4998–5005 (2010).
[5]J. A. Ng, J. T. Booth, P. R. Poulsen, W. Fledelius, E. S. Worm, T. Eade, F. Hegi, A. Kneebone, Z. Kuncic, and P. J. Keall, "Kilovoltage intrafraction monitoring for prostate intensity modulated arc therapy: First clinical results," Int. J. Radiat. Oncol., Biol., Phys. **84**(5), e655–e661 (2012).
[6]T. P. O'Shea, L. J. Garcia, K. E. Rosser, E. J. Harris, P. M. Evans, and J. C. Bamber, "4D ultrasound speckle tracking of intra-fraction prostate motion: A phantom-based comparison with x-ray fiducial tracking using CyberKnife," Phys. Med. Biol. **59**(7), 1701–1720 (2014).
[7]T. P. O'Shea, J. C. Bamber, D. Fontanarosa, S. van der Meer, F. Verhaegen, and E. J. Harris, "Review of ultrasound image guidance in external beam radiotherapy part 2: Intra-fraction motion management and novel applications," Phys. Med. Biol. **61**(8), R90–R137 (2016).
[8]M. F. Fast, S. Nill, J. L. Bedford, and U. Oelfke, "Dynamic tumor tracking using the Elekta agility MLC," Med. Phys. **41**(11), 111719 (5pp.) (2014).
[9]M. Lachaine and T. Falco, "Intrafractional prostate motion management with the clarity autoscan system," Med. Phys. Int. **1**(1), 72–80 (2013).
[10]J. L. Bedford, M. F. Fast, S. Nill, F. M. McDonald, M. Ahmed, V. N. Hansen, and U. Oelfke, "Effect of MLC tracking latency on conformal volumetric modulated arc therapy (VMAT) plans in 4D stereotactic lung treatment," Radiother. Oncol. **117**(3), 491–495 (2015).
[11]G. Davies, P. Clowes, J. Bedford, P. Evans, S. Webb, and G. Poludniowski, "An experimental evaluation of the Agility MLC for motion-compensated VMAT delivery," Phys. Med. Biol. **58**(13), 4643–4657 (2013).
[12]A. Krauss, S. Nill, and U. Oelfke, "The comparative performance of four respiratory motion predictors for real-time tumour tracking," Phys. Med. Biol. **56**(16), 5303–5317 (2011).
[13]J. L. Bedford, Y. K. Lee, P. Wai, C. P. South, and A. P. Warrington, "Evaluation of the Delta[4] phantom for IMRT and VMAT verification," Phys. Med. Biol. **54**(9), N167–N176 (2009).
[14]E. J. Harris, N. R. Miller, J. C. Bamber, J. R. N. Symonds-Tayler, and P. M. Evans, "The effect of object speed and direction on the performance of 3D speckle tracking using a 3D swept-volume ultrasound probe," Phys. Med. Biol. **56**(22), 7127–7143 (2011).
[15]N. Otsu, "A threshold selection method from gray-level histograms," IEEE Trans. Syst. Man Cybernet. **9**(1), 62–66 (1979).
[16]L. R. Dice, "Measures of the amount of ecologic association between species," Ecology **26**(3), 297–302 (1945).
[17]W. Fledelius, P. J. Keall, B. Cho, X. Yang, D. Morf, S. Scheib, and P. R. Poulsen, "Tracking latency in image-based dynamic MLC tracking with direct image access," Acta Oncol. **50**(6), 952–959 (2011).
[18]M. A. L. Bell, B. C. Byram, E. J. Harris, P. M. Evans, and J. C. Bamber, "*In vivo* liver tracking with a high volume rate 4D ultrasound scanner and a 2D matrix array probe," Phys. Med. Biol. **57**(5), 1359–1374 (2012).